

Ultra light-trapping filters with broadband reflection holograms

Deming Zhang,^{1,*} Shelby Vorndran,² Juan M. Russo,¹ Michael Gordon,²
and Raymond K. Kostuk^{1,2}

¹Electrical and Computer Engineering Department, University of Arizona, 1230 E Speedway Boulevard, Tucson, Arizona 85721, USA

²College of Optical Sciences, University of Arizona, 1630 East University Boulevard, Tucson, Arizona 85721, USA
[*dzhang@email.arizona.edu](mailto:dzhang@email.arizona.edu)

Abstract: Significant optical absorption enhancement can be achieved by incorporating optical diffusers in the thin-film silicon photovoltaic (PV) cells. Absorption can be increased further by angular and spectral selective filters. In this work the properties of volume reflection holograms are examined for realizing ultra light-trapping filters for thin film silicon photovoltaic cell applications. The filter properties of reflection volume hologram are evaluated for this application. It is found that variation in the refractive index profile as a function of depth is an important factor. The optimized design is implemented in dichromated gelatin holograms and found to be in good agreement with predicted performance. The enhancement to the conversion efficiency of silicon PV cells are predicted with the PC-1D simulation tool and is found to be similar to that with an optimized Rugate filter. The simulated short circuit current density enhancement was found to be 8.2% for a 50 μm thick silicon PV cell and 15.8% for a 10 μm thick silicon PV cell.

©2012 Optical Society of America

OCIS codes: (090.2890) Holographic optical elements; (310.0310) Thin films; (040.5350) Photovoltaic; (350.6050) Solar energy.

References and links

1. E. Yablonovitch and G. D. Cody, "Intensity enhancement in textured optical sheets for solar cells," *IEEE Trans. Electron. Dev.* **29**(2), 300–305 (1982).
2. S. Fahr, C. Ulbrich, T. Kirchartz, U. Rau, C. Rockstuhl, and F. Lederer, "Rugate filter for light-trapping in solar cells," *Opt. Express* **16**(13), 9332–9343 (2008).
3. J. C. Miñano, "Optical confinement in photovoltaics," *Physical Limitations to the Photovoltaic Solar Energy Conversion* (Hilger, 1990).
4. C. Ulbrich, S. Fahr, J. Üpping, M. Peters, T. Kirchartz, C. Rockstuhl, R. Wehrspohn, A. Gombert, F. Lederer, and U. Rau, "Directional selectivity and ultra-light-trapping in solar cells," *Phys. Status Solidi* **205**(12), 2831–2843 (2008) (a).
5. M. Peters, J. C. Goldschmidt, T. Kirchartz, and B. Bläsi, "The photonic light trap—Improved light trapping in solar cells by angularly selective filters," *Sol. Energy Mater. Sol. Cells* **93**(10), 1721–1727 (2009).
6. P. G. Boj, J. Crespo, and J. A. Quintana, "Broadband reflection holograms in dichromated gelatin," *Appl. Opt.* **31**(17), 3302–3305 (1992).
7. T. Jansson, I. Tenggara, Y. Qiao, and G. Savant, "Lippmann-Bragg broadband holographic mirrors," *J. Opt. Soc. Am. A* **8**(1), 201–211 (1991).
8. C. G. Stojanoff, "Review of the technology for the manufacturing of large-format DCG holograms for technical applications," *Proc. SPIE* **3011**, 267–278 (1997).
9. J. Jansson, T. Jansson, and K. H. Yu, "Solar control tunable Lippmann holowindows," *Sol. Energy Mater.* **14**(3-5), 289–297 (1986).
10. S. Case and R. Alferness, "Index modulation and spatial harmonic generation in dichromated gelatin films," *Appl. Phys. A-Mater.* **10**, 41–51 (1976).
11. T. Kubota, "Control of the reconstruction wavelength of Lippmann holograms recorded in dichromated gelatin," *Appl. Opt.* **28**(10), 1845–1849 (1989).
12. W. H. Southwell, "Extended-bandwidth reflector designs by using wavelets," *Appl. Opt.* **36**(1), 314–318 (1997).
13. W. H. Southwell, "Using apodization functions to reduce sidelobes in rugate filters," *Appl. Opt.* **28**(23), 5091–5094 (1989).

14. Z. N. Kalyashova, E. V. Kalyashov, G. A. Cheremisina, and D. I. Matveeva, "Intensive Bragg harmonics in reflection holograms in dichromated gelatin: II," Proc. SPIE **3011**, 279–284 (1997).
 15. T. K. Gaylord and M. G. Moharam, "Analysis and applications of optical diffraction by gratings," Proc. IEEE **73**(5), 894–937 (1985).
 16. M. A. Green and M. J. Keevers, "Optical properties of intrinsic silicon at 300 K," Prog. Photovolt. Res. Appl. **3**(3), 189–192 (1995).
 17. M. A. Green, "Lambertian light trapping in textured solar cells and light-emitting diodes: analytical solutions," Prog. Photovolt. Res. Appl. **10**(4), 235–241 (2002).
 18. P. A. Basore, "Numerical modeling of textured silicon solar cells using PC-1D," IEEE Trans. Electron. Dev. **37**(2), 337–343 (1990).
-

Introduction

Light-trapping in photovoltaic (PV) cells increases the effective optical path-length in the semiconductor material leading to greater absorption and conversion efficiency. One approach to produce light trapping is by incorporating a diffuse layer on the surface of the cell. This can change the direction of the rays that enter the cell medium forcing some of the rays to exceed the critical angle of the cell/air interface. The portion of rays that exceed the critical angle are trapped in the cell by total internal reflection (TIR) leading to longer optical path length and greater absorption in the cell. It has been shown that the effective optical path length can be increased by a factor of $4n^2$ using diffusive surfaces on a PV cell. For silicon with a refractive index of 3.7 at near-infrared wavelength an enhancement factor of 55 can be realized [1]. This leads to a considerable reduction of PV material while maintaining approximately the same electrical output power.

Recently it has been shown that the $4n^2$ path length and absorption enhancement can be further improved with the addition of angular and wavelength selective filters to the diffuser surface [2–4]. The filter decreases the escape cone for rays within the substrate providing a greater light-trapping effect. The filter-diffuser combination increases the effective optical path length by a factor of $4n^2/\sin^2\theta$ [3], where θ is the ideal half-angle of the escape cone in air.

Ultra light-trapping filters have previously been realized with dielectric multi-layer stacks [5]. A maximum of 25% increase in monochromatic absorption was demonstrated and the efficiency improvement under AM1.5 spectrum was 5.5% [5]. A broadband dielectric Rugate coating was also designed for light trapping and a 4.87% increase in efficiency was found due to light-trapping [2]. The Rugate coating was optimized with a continuously varying refractive index profile in the depth direction by assuming a co-deposition fabrication process [2]. Both approaches are limited by relatively high production costs which constrain their use in mass production.

Dichromated Gelatin (DCG) holograms exhibit large refractive index modulation on the order of 0.1. DCG holograms can record interference fringes with spatial frequency as high as 5000 lines/mm and large scale production capability has been demonstrated [6–8]. DCG reflection holograms formed in the Lipmann geometry show strong specular reflection properties. Holograms of this type have been fabricated for sunlight control [7,9] and solar concentration [8] purposes. Therefore DCG holographic filter can be a possible low cost counterpart to more expensive dielectric multi-layer and Rugate filter implementations.

In this paper, the light-trapping properties of broadband reflection holograms are analyzed. The diffraction efficiency characteristics of broadband reflection hologram are designed to achieve light-trapping in silicon thin-film PV cells. Diffraction properties of broadband reflection holograms are modeled using rigorous coupled wave analysis taking into account the depth variation in refractive index profile. A simplified procedure is described to produce broadband reflection holograms. Modeling parameters are extracted from prototype DCG holograms and good matches are found between simulation and experiment at diffraction properties. The absorption enhancement factor for a thin film silicon PV cell is predicted with the PC-1D simulation program. The absorption enhancement factor obtained with a DCG holographic filter was found to be similar to that of an optimum Rugate filter. The

enhancement in short circuit current density was found to be 8.2% for a 50 μm thick silicon PV cell and 15.8% for a 10 μm thick silicon PV cell.

Light trapping with reflection holographic filter

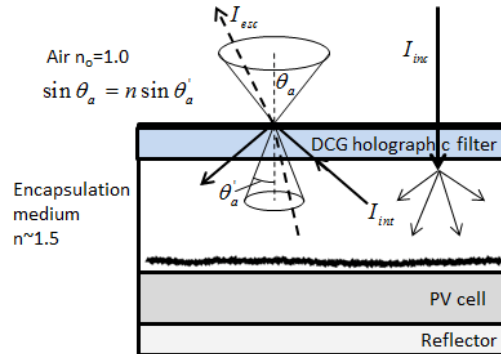


Fig. 1. Typical light-trapping structure. A DCG holographic filter is included in a regular PV encapsulation. The escape cone in air has half-angle of θ_a and the corresponding half-angle in the encapsulation medium is θ'_a .

The geometry for realizing the ultra light-trapping filter is shown in Fig. 1. A dichromated gelatin holographic filter and diffuser are encapsulated with the PV cell and a back reflector. At normal incidence the DCG holographic filter has high transmittance in the 400 nm to 1100 nm wavelength range. Light is randomly distributed into all directions by the diffuser and reflected back to the holographic filter by the back reflector. The filter only allows light to escape the structure within the loss cone shown in Fig. 1 with a half angle of θ_a . The corresponding half angle in the encapsulation medium is θ'_a . Light outside of the loss cone is trapped by the holographic filter. It has been shown that the absorption enhancement factor for this system can be $4n^2 / \sin^2 \theta_a$ if the loss cone has a half angle of θ_a [3].

The properties of an ideal light-trapping holographic filter are shown in Fig. 2. The grating fringes are parallel with the surface of the substrate. The filter follows the Bragg matching condition [Eq. (1)] over a range of angles of incidence and wavelengths. In the ideal case incident light is diffracted between the curved band sections in the middle of the graph and transmitted elsewhere. At normal incidence, the transmittance is unity for usable light in the PV cell ($\lambda < 1.0 \mu\text{m}$). At larger angles of incidence the high reflectivity wavelength becomes shorter as predicted by the Bragg condition. Incident photons with energy close to the bandgap of silicon are reflected by the hologram at large angles and trapped within the solar cell. The boundaries for reflection as a function of the incident angle and wavelength are modeled with the Bragg condition:

$$\lambda_p(\theta) = 2\Lambda\sqrt{(n^2 - \sin^2 \theta)} \quad (1)$$

where n is the refractive index of the medium, θ is the angle of incidence and Λ is the grating period.

The mechanism for trapping long wavelength light using a perfect Bragg filter is illustrated in Fig. 2. The two curves in Fig. 2(a) show the boundaries for reflection as a function of the incident angle and wavelength in air. Solar illumination between λ_{short} and λ_{long} are incident on the ultra-filter/diffuser/PV cell as shown in the figure at near normal incident angles. The light passes through the hologram and is then scattered by the diffuser increasing the propagation angle in the substrate. For the example in Fig. 2(b) if light is scattered with an angle of 40° the short wavelength light (900 nm) will be transmitted by the hologram while

the longer wavelength light (1000 nm) is reflected by the hologram and trapped. At a 60° scatter angle light with wavelengths between 900 nm and 1000 nm is diffracted by the hologram back into the substrate where it will propagate through the PV cell and increase the probability of absorption. As a result of the perfect Bragg reflection filter, light that satisfies the conditions in the dashed region in Fig. 2(a) is trapped by the holographic filter after randomized scattering. More light-trapping benefit is achieved at longer wavelength at the cost of more restricted acceptance angle.

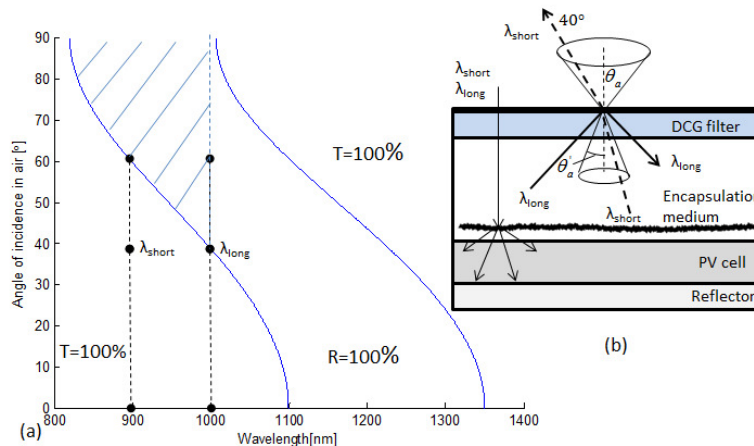


Fig. 2. Optical transmittance of an ideal Bragg light-trapping filter: (a) the high reflection spectral bands at different ray angles in air; (b) diagram of ray transmission and reflection.

Properties of broadband reflection holograms

In order to function effectively as ultra light-trapping filters, the volume reflection holograms must have high diffraction efficiency over a broad spectral range. In addition they must diffract with high efficiency at large angles of incidence and be transparent at angles less than the system acceptance angle. The diffraction efficiency of the hologram is defined as: $\eta(\lambda, \theta) = I_{dif}(\lambda, \theta) / I_{inc}(\lambda, \theta)$, where $I_{inc}(\lambda, \theta)$ and $I_{dif}(\lambda, \theta)$ are the incident and diffracted optical power.

Sensitized dichromated gelatin (DCG) holograms exhibit high refractive index modulation, broad range of linear sensitivity, low scattering and low absorption [6–8,10]. It is also possible to chirp or vary the grating period as a function of thickness [6,8,11,12]. The grating chirp increases the spectral and angular bandwidth of the grating. Refractive index apodization can also be realized in DCG hologram which is useful for controlling the strength of side lobes in the diffraction efficiency response [6,11,13]. In addition, once sealed in a manner similar to PV modules, they have excellent long term stability properties.

DCG holographic films can be made with a variety of coating techniques. In our lab a sensitized gelatin mixture was spin-coated onto a glass substrate. The sensitized gelatin mixture consists of 20% gelatin solution in de-ionized water, and is sensitized with 2% ammonium dichromate by weight to water. The solution temperature is maintained at 40°C before spin-coating and a constant air flow is supplied over the coating substrate while maintaining the temperature at 40°C. After 5 minutes of spin-coating at 125 rotations per minute (RPM), the plates were removed from the spinner and allowed to dry for an hour in an environment with 25°C and 45% RH. The plates are then baked for 45 minutes at 90°C and cooled down to 25°C. This process yields a DCG film with a thickness of 17 μm as measured with a Filmetrics system and the average refractive index was found to be 1.53 as determined with the Brewster angle method. The shelf life of such plates is usually 2 weeks in light-tight containers under room temperature and 15% relative humidity.

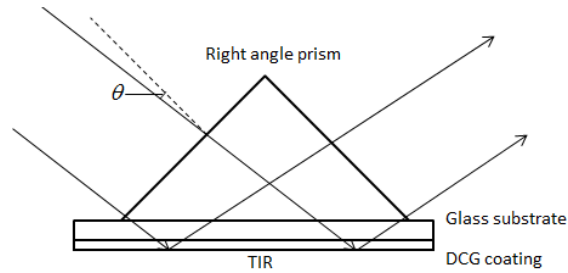


Fig. 3. Exposure geometry for reflection DCG holographic filter.

The DCG film is exposed using a collimated argon ion laser beam at 514 nm through a right angle prism as shown in Fig. 3. The right-angle prism is used to achieve large incident angle in the medium. The central reflection peak is controlled by changing the incident angle of the construction beam as shown in Fig. 3. A larger incident angle gives longer central wavelength. The incident angle θ (Fig. 3) was 22° in air relative to the prism side surface normal. The uncoated side of the DCG plate is index matched with Xylene to the hypotenuse face of the prism. The interference pattern formed between the incident and TIR beams is recorded during the exposure. Using this setup the interference fringes are parallel to the surface of the film. The spectral bandwidth is controlled by fine-tuning exposure energy, isopropanol development temperature and hardening time in the fixer bath. The optimum exposure flux density is approximately 147 mJ/cm^2 . Higher exposure energy will increase high order harmonics in the diffraction efficiency due to non-linear behavior in light sensitivity [10,14]. The development procedure is described in Table 1 and the time interval between the exposure and development is kept to a minimum (less than 5 minutes).

Table 1. DCG Development Procedure

1. Fix plate in 25°C Kodak Rapid Fixer for 120 seconds
2. Rinse in 20°C de-ionized water for 30 seconds
3. Wash with 25°C 50% isopropanol (50% de-ionized water) for 30 seconds
4. Wash with 25°C 75% isopropanol for 30 seconds
5. Dehydrate with 25°C 99% isopropanol for 30 seconds
6. Bake in 75°C oven for 20 minutes

The diffraction efficiency of the resulting holograms is obtained by measuring the transmittance spectrum. The spectral transmittance is the ratio of the transmitted spectral flux of the hologram and that of an uncoated glass substrate. The measured transmittance of a prototype hologram is shown in Fig. 4. Transmission of short wavelength visible light is slightly reduced due to scattering in the hologram. Two small rejection peaks can be seen in the visible spectrum at 410 nm and 600 nm. These are indications of the second and third order harmonics in the refractive index modulation profile. The hologram illustrated in Fig. 4 has not been completely optimized for reducing higher order harmonic reflection. However the secondary order at near 610 nm is relatively weak and the third order near 400 nm falls within the spectral region where the silicon PV cells do not have strong spectral responsivity. In addition techniques for further reduction of higher order reflections by controlling exposure and development condition can also be applied to reduce these effects. The experimental hologram exhibits isotropic scattering that account for about 8% losses in transmittance. The scattering is not desired because part of the light enters back scattering and do not reach the PV cell. The calculated backscattered light which does not enter the medium is 1.7%. This scattering can be further minimized by careful control of the hologram development procedure. Therefore due to the low lost back scattered component in the following simulation it is assumed the scattering does not create significant effects.

The diffraction efficiency is $DE(\lambda) = 1 - T(\lambda) - E(\lambda)$, where $T(\lambda)$ and $E(\lambda)$ are the spectral transmittance and spectral extinction respectively. In the unslanted reflection configuration in

Fig. 3, the diffraction efficiency is equal to the reflectance since all the diffracted orders follow the specular reflection angle. The spectral extinction accounts for both absorption and scattering losses. Holograms with extremely low absorption and scattering losses have been experimentally shown in [8].

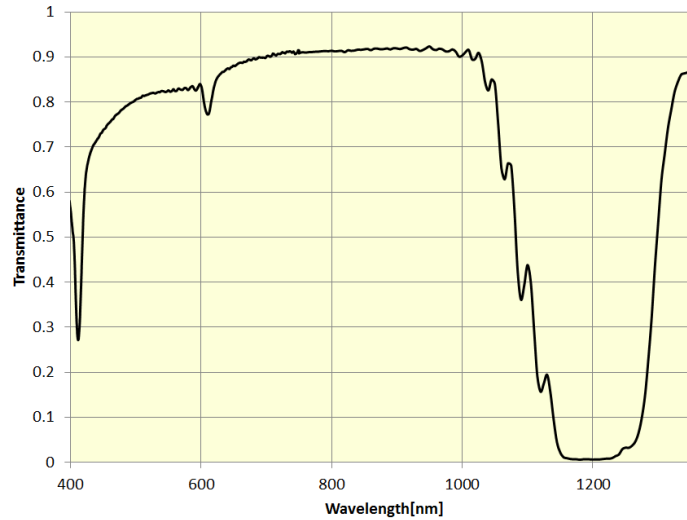


Fig. 4. Measured specular transmittance of an experimental DCG filter at normal incidence.

Rigorous Coupled Wave (RCW) analysis [15] can accurately model non-uniform grating modulation profile as well as the grating period chirp and apodization as functions of depth. The refractive index modulation and the grating period profiles can be approximated by the following equations [6,11]:

$$n_1(z) = n_1(d) - \Delta n_1 \left(1 - \frac{z}{d}\right)^r \quad (2)$$

$$\Lambda(z) = \Lambda(0) - \Delta\Lambda \left(\frac{z}{d}\right)^s \quad (3)$$

where z is distance from the hologram/glass interface and d is the total thickness of the hologram. The parameters “ r ” and “ s ” are empirically determined constants. The refractive index modulation is highest at the hologram/air surface and the grating period is largest at the hologram/glass interface. The value of $n_1(d)$ and $\Lambda(0)$ are the corresponding refractive index modulation and grating period maxima. Grating parameters d , n_1 , Δn_1 , $\Lambda(0)$, $\Delta\Lambda$, r and s are varied in the model to find the best fit to the experimentally obtained diffraction efficiency data. The best fit parameters are shown in Table 2. Both the simulated and measured diffraction efficiency curves are plotted in Fig. 5. The measured diffraction efficiency is indirectly obtained from the spectral transmittance.

Table 2. Best-Fit Parameters for the Experimental DCG Holographic Filter

d	n_1	Δn_1	$\Lambda(0)$	$\Delta\Lambda$	r	s
17 μm	0.125	0.0437	0.41 μm	0.0193 μm	3	2

The RCW simulated diffraction efficiency as both functions of wavelength (x-axis) and angle (y-axis) is shown in Fig. 6. The angle of incidence is evaluated in the grating medium. The diffraction efficiency of both TE and TM polarizations are averaged to give the diffraction efficiency of unpolarized light. The blue shift of the high diffraction efficiency band matches previous predictions using the Bragg conditions. It can be seen that both the

peak value and the bandwidth of the diffraction efficiency are reduced at large angles of incidence. It is not necessary to optimize the diffraction efficiency at incident angles that is larger than the critical angle since they undergo total internal reflection and are trapped. The critical angle is around 41° in the medium when the refractive index of the encapsulation medium is 1.53.

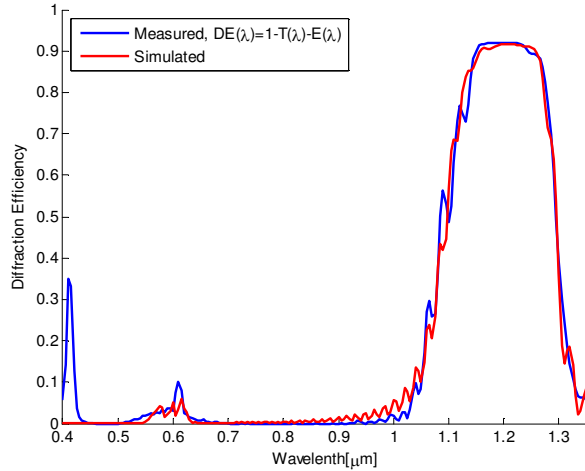


Fig. 5. Measured (blue) and simulated (red) diffraction efficiency characteristics.

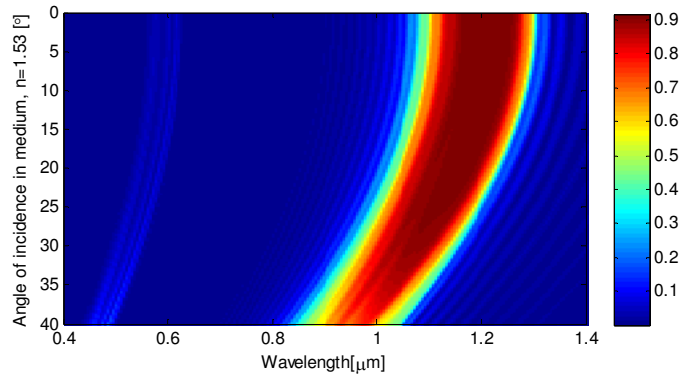


Fig. 6. Simulated diffraction efficiency for a range of angle of incidence and wavelength. The angle of incidence is evaluated in the grating medium ($n = 1.53$). Parameters used for the simulation are listed in Table 2.

PV cell absorption enhancement

The holographic filter allows light at all wavelengths to enter the light trapping structure at angles less than the acceptance angle θ_a . The filter also reflects light for $\theta' > \theta_a'$ at specific wavelength λ . The angles θ' and θ_a' are within the encapsulation medium which is assumed to be index matched with the holographic grating. Using these properties, the absorption enhancement factor for a filter of this type used in a light trapping configuration as in Fig. 1 can be specified as [1]:

$$k = \frac{2 \cdot T(0^\circ, \lambda)}{\int_0^{\pi/2} T(\theta, \lambda) \cos \theta \sin \theta d\theta} \quad (4)$$

in which $T(\theta, \lambda)$ is the spectral transmittance of the filter at angle of incidence θ and wavelength λ . This equation assumes that the optical diffuser has the same refractive index as the hologram, the PV cell material is weakly absorbing and the Fresnel reflection losses are negligible. The angle θ is evaluated in the hologram medium with a refractive index of 1.53. The spectral transmittance is taken to be $T(\theta, \lambda) = 1 - DE(\theta, \lambda)$ when the ray angle is less than the critical angle. $T(0^\circ, \lambda)$ is the spectral transmittance at normal incidence. The transmittance is zero at angles larger than the critical angle ($\sim 41^\circ$) in the medium due to total internal reflection.

The above equation is evaluated numerically using the experimental data from the reflection holographic filter (Fig. 6) and the resulting absorption enhancement factor is shown in Fig. 7. There is an almost constant absorption enhancement for wavelength shorter than 850 nm due to the diffuser. From 800nm to 1100nm, the absorption enhancement increases as a result of light trapping by the holographic filter. The enhancement drops down for $\lambda > 1.1 \mu\text{m}$ due to limit in the filter transmittance. Overall, the large absorption enhancement in the 800 nm to 1100 nm wavelength range can provide significantly improvement in light absorption at the band edge of silicon.

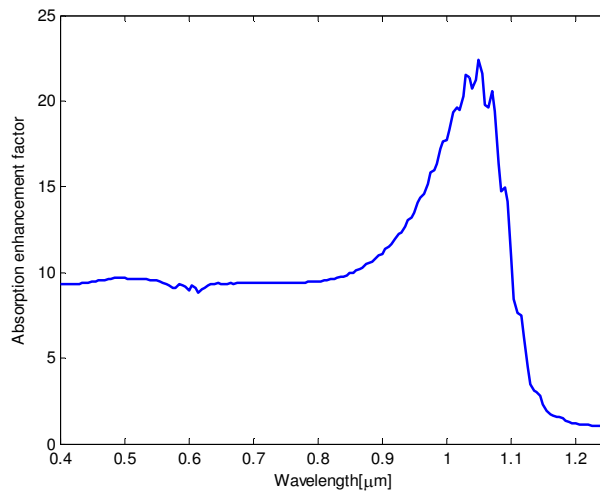


Fig. 7. Absorption enhancement factor calculated numerically using DE properties shown in Fig. 6.

The one-dimensional carrier generation profile $g(\lambda, z)$ is defined as: $g(\lambda, z) = N(\lambda, z) / N_p(\lambda)$, in which $N_p(\lambda)$ is the rate of photon incidence and $N(\lambda, z)$ is the photon absorption rate per unit depth at wavelength λ . The absorption coefficient $\alpha(\lambda)$ for a silicon PV cell at wavelength λ is assumed [16]. The spectral absorption is related to the generation profile $g(\lambda, z)$ for wavelength λ at depth z given by:

$$A(\lambda) = \int_{z=0}^d g(\lambda, z) dz \quad (5)$$

with d being the total thickness of the PV material.

The carrier generation profile for a double-side polished PV cell with thickness d and an ideal back reflector is given by:

$$g_0(\lambda, z) = \alpha(\lambda) \cdot (e^{-\alpha(\lambda) \cdot z} + e^{\alpha(\lambda) \cdot (z-2d)}) \quad (6)$$

and the total absorption in this configuration is:

$$A_0(\lambda) = 1 - e^{-2\alpha(\lambda)d} \quad (7)$$

The carrier generation profile for a PV cell and back reflector with a Lambertian diffuser is [17]:

$$g_1(\lambda, z) = 2\alpha(\lambda) \cdot \frac{Ei_2(\alpha(\lambda) \cdot z) + Ei_2(\alpha(\lambda) \cdot (2d - z))}{1 - t_{cell} [1 - t_{diffuser}(\lambda)]} \quad (8)$$

in which $t_{diffuser} = 1/n^2$ [4,17] with n being the refractive index of the encapsulation medium. t_{cell} is the transmittance averaged for all possible angles of incidence for light making a round trip from front to rear and back [17]:

$$t_{cell}(\lambda) = \frac{1 - \alpha(\lambda) \cdot 2d}{e^{\alpha(\lambda) \cdot 2d}} + [\alpha(\lambda) \cdot 2d]^2 \cdot Ei(\alpha(\lambda) \cdot 2d) \quad (9)$$

and Ei(z) is the exponential integral defined as $Ei(z) = \int_z^\infty \frac{e^{-t}}{t} dt$.

The corresponding total absorption for a specular PV cell with a Lambertian diffuser is:

$$A_1(\lambda) = \frac{1 - t_{cell}(\lambda)}{1 - t_{cell}(\lambda) [1 - t_{diffuser}(\lambda)]} \quad (10)$$

When an additional broadband reflection hologram is included, the photon generation profile changes to [4,17]:

$$g_2(\lambda, z) = 2\alpha(\lambda) \cdot \frac{Ei_2(\alpha(\lambda) \cdot z) + Ei_2(\alpha(\lambda) \cdot (2d - z))}{1 - t_{cell} (1 - t_{diffuser, filter})} \quad (11)$$

And the corresponding absorption is given by:

$$A_2(\lambda) = \frac{1 - t_{cell}(\lambda)}{1 - t_{cell}(\lambda) [1 - t_{diffuser, filter}(\lambda)]} \quad (12)$$

The parameter $t_{diffuser, filter}(\lambda)$ is defined as the angular integrated transmittance of both the diffuser and the holographic filter. This parameter is evaluated numerically with simulated diffraction efficiency using RCW method:

$$t_{diffuser, filter}(\lambda) = \frac{\int_0^{\pi/2} [1 - DE(\lambda, \theta)] \sin \theta \cos \theta d\theta}{\int_0^{\pi/2} \sin \theta \cos \theta d\theta} \quad (13)$$

where $DE(\lambda, \theta)$ is the diffraction efficiency of the holographic filter and the exponential

integral $Ei_2(z)$ is: $Ei_2(z) = z \int_z^\infty \frac{e^{-t}}{t^2} dt$.

The spectral absorption for silicon PV cells for the three different configurations are calculated and shown in Fig. 8. When the PV cell thickness is 50 μm , the absorption enhancement due to the holographic filter extends the usable spectral range from 1000 nm to about 1100 nm. The enhancement is more significant for the 10 μm thick Si PV cell. The

thinner Si cell with 10 μm thickness cannot effectively absorb light past 900 nm. However the same cell incorporated with diffuser and holographic filter can absorb effectively up to 1050 nm.

Some additional reflection losses introduced by the holographic filter limit the overall absorption past 1150 nm for both 10 μm and 50 μm thick PV cells. However the loss in energy conversion is negligible since the spectral responsivity of silicon is extremely low at larger wavelength.

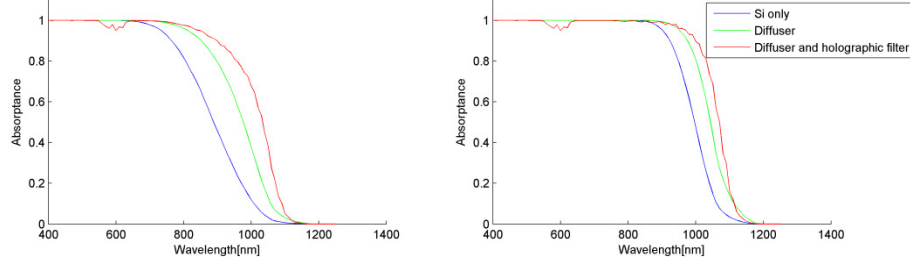


Fig. 8. Simulated absorbance for silicon solar cells with thickness of 50 μm (left) and 10 μm (right).

The total carrier generation rate as a function of depth under standard AM1.5 direct illumination is numerically obtained by integrating over the responsive wavelength range:

$$G(z) = \int_{\lambda=400\text{nm}}^{1200\text{nm}} N_{p,AM1.5}(\lambda) \cdot g(\lambda, z) d\lambda \quad (14)$$

where $N_{p,AM1.5}(\lambda)$ is the photon incident rate under the AM 1.5 direct spectrum. It can be calculated as $N_{p,AM1.5}(\lambda) = \lambda E_{AM1.5}(\lambda) / hc$ in which the $E_{AM1.5}(\lambda)$ is the spectral optical power incident on the PV cell, h is the Planck's constant and c is the speed of light in vacuum and $g(\lambda, z)$ is the normalized spectral generation rate at depth z in the PV cell.

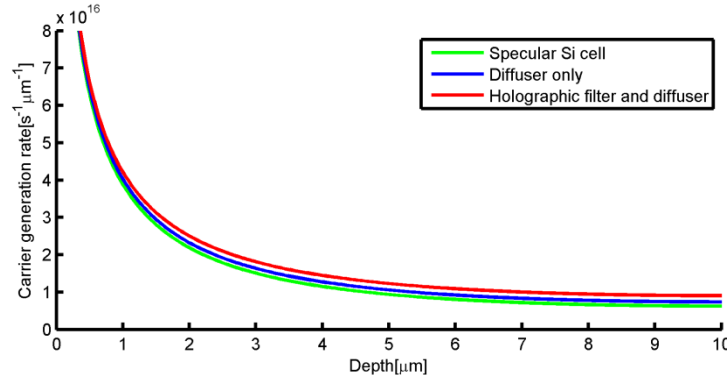


Fig. 9. The total carrier generation rate for a 10 μm thick specular thin-film silicon PV cell, cell with Lambertian diffuser and with both diffuser and holographic filter.

With the 10 μm thick Si cell, the total carrier generation rate is calculated for the three cases including bare specular cell, specular cell with Lambertian diffuser, and specular cell with diffuser and holographic filter and is plotted in Fig. 9. The Lambertian diffuser provides a noticeable improvement in carrier generation in the PV medium and further improvement is introduced with the additional holographic filter, as can be seen in Fig. 9.

The carrier collection characteristics over the depth of the PV cell are modeled using the PC-1D software [18]. The computation is performed using the carrier generation rate profile

from the analytical expressions [Eqs. (6), (8) and (11)] and the thin film silicon PV cell parameters shown in Table 3.

The simulated IV curves are shown in Fig. 10. The specular cell with thickness of 10 μm has a short circuit current density of 29.7 mA/cm^2 and a higher short circuit current density of 31.6 mA/cm^2 is achieved with the addition of a Lambertian diffuser (Fig. 9), which is a 6.4% improvement. The highest generation rate is obtained by the cell that has diffuser and holographic filter. The corresponding current density is 34.4 mA/cm^2 resulting from an 8.9% improvement compared to the same PV cell with only the diffuser and a 15.8% improvement compared to bare specular cell.

Table 3. Parameters of Thin-Film Silicon Solar Cell used in PC-1D Simulation

Exterior Front Reflectance	10%
Thickness	10 μm , 50 μm
Intrinsic carrier concentration	$1 \times 10^{10} \text{ cm}^{-3}$
P-type background doping	$1.5 \times 10^{16} \text{ cm}^{-3}$
Front diffusion N-type doping	$2 \times 10^{20} \text{ cm}^{-3}$, with erfc distribution peak at top surface, depth factor is 0.1 μm
Carrier lifetime	5 μs
Front surface recombination velocity	$S_n = S_p = 1000 \text{ cm/s}$
Rear surface recombination velocity	$S_n = S_p = 500 \text{ cm/s}$

For a 50 μm thick silicon cell, a bare specular cell is capable of generating a short circuit current density of 36.5 mA/cm^2 . The performance improves by 3.0% to 37.6 mA/cm^2 with the optical diffuser and with both the diffuser and the holographic filter, the performance increases by 8.2% to 39.5 mA/cm^2 compared to the specular case.

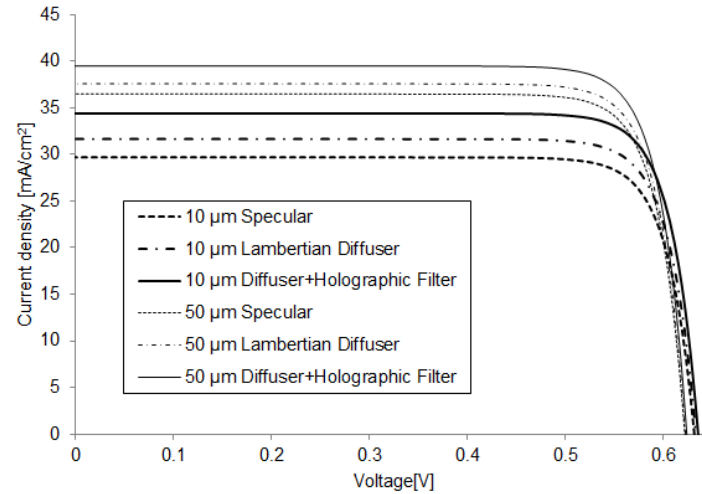


Fig. 10. Simulated IV curves for 10 μm and 50 μm Si PV cells with different light trapping configurations.

Conclusions

In this paper holographic reflection gratings have been shown to function as ultra-light trapping filters for enhancing the performance of thin film PV cells. Results from an experimental reflection hologram were used to model the absorption enhancement factor for a silicon solar cell and light trapping filter. The result shows an increase in this factor by nearly 23% over the PV cell without the light trapping filter. The experimental holographic filter

properties were also incorporated into the PC-1D simulation tool to model the short circuit current density. The result of this simulation shows an improvement of 8.2% for a 50 μm thick silicon PV cell and a 15.8% improvement for a 10 μm thick cell. The holographic filter has the advantage that it is separate from the PV cell and does not require modification of the PV cell surface which can decrease electrical performance. In addition holographic filters can be fabricated in large areas at low cost making it a viable technique for cost effective PV systems.